Analysing dynamical disorder for charge transport in organic semiconductors via machine learning

Patrick Reiser[1,2], Manuel Konrad[1], Artem Fediai[1], Salvador Léon[3], Wolfgang Wenzel[1] and Pascal Friederich[1,2,]*

[1]Institute of Nanotechnology, Karlsruhe Institute of Technology (KIT), Hermann-von-Helmholtz-Platz 1, 76344 Eggenstein-Leopoldshafen,Germany
[2]Institute of Theoretical Informatics, Karlsruhe Institute of Technology (KIT), Am Fasanengarten 5, 76131 Karlsruhe, Germany
[3]Department of Industrial Chemical Engineering and Environment, Universidad Politécnica de Madrid, C/ José Gutierrez Abascal, 2, 28006 Madrid, Spain

Molecule (HOMO)	Mean total [eV]	Disorder static [meV]	Disorder dynamic [meV]	Disorder total [meV]
a-NPD	-5.04	20	102	110
B4PyMPM	-6.75	11	97	99
B4PyPPM	-6.69	14	86	87
m-BPD	-4.95	61	79	93
mCP	-5.51	16	63	65
NPB	-5.17	40	95	106
o-BPD	-5.25	28	88	94
p-BPD	-4.92	68	77	92
Spiro-OMeTAD	-4.50	56	86	102
Spiro-TAD	-4.73	37	72	83
TCTA	-5.34	71	89	109
TPBi	-5.91	24	71	78
TPyQB	-6.28	42	79	82

Table S1: *HOMO values for central peak and disorder, extracted from 6 DFT reference geometries.*

Molecule (LUMO)	Mean total [eV]	Disorder static [meV]	Disorder dynamic [meV]	Disorder total [meV]
a-NPD	-1.52	26	99	100
B4PyMPM	-2.09	89	113	149
B4PyPPM	-2.13	113	112	142
m-BPD	-1.23	111	135	153
mCP	-1.27	14	93	112
NPB	-1.56	30	95	99
o-BPD	-1.21	105	127	151
p-BPD	-1.25	107	128	157
Spiro-OMeTAD	-1.31	56	104	135
Spiro-TAD	-1.49	47	108	132
TCTA	-1.61	113	128	177
TPBi	-1.46	35	118	136
TPyQB	-2.09	41	80	91

Table S2: *LUMO values for central peak and disorder, extracted from 6 DFT reference geometries.*

Short discussion on ML error and disorder prediction:

It is to note that an ML model will also have an uncertainty σ_{ML} that will affect the ML-predicted disorder values for the dynamic σ_d and total disorder σ_t. If the ML model was not biased, the predicted disorder distribution would be homogeneously broadened in comparison to the actual energy distribution. However, if the prediction error was further uncorrelated and approximately normally distributed, the ML-uncertainty adds quadratically to the actual disorder $\sigma_d(ML)^2 = \sigma_d^2 + \sigma_{ML}^2$. As a consequence, the ML error has to be smaller than the disorder under consideration. If we take, for example $\sigma_{ML} = \alpha\,\sigma_d$ and $\alpha = 0.3$, the predicted disorder is overestimated by $\sigma_d(ML) = \sigma_d\sqrt{\alpha^2 + 1} = 1.04\,\sigma_d$. In the case of a Gaussian probability distribution, the standard deviation σ is related to the mean absolute deviation by $MAE = E[|X - E[X]|] = \sigma\sqrt{2/\pi}$, which is usually given as a metric in machine learning models.

Molecule (HOMO)	Mean absolute error [meV]	r^2	Disorder static [meV]	Disorder dynamic [meV]	Disorder total [meV]	Squared Sum of dynamic and static disorder [meV]
a-NPD	17	0.96	35.0	104.0	109.7	109.7
B4PyMPM	29	0.85	14.4	91.7	92.8	92.8
B4PyPPM	36	0.69	16.2	80.4	82.0	82.0
m-BPD	17	0.95	50.5	76.0	91.3	91.3
mCP	9	0.96	20.0	62.1	65.2	65.2
NPB	15	0.97	53.5	90.4	105.0	105.0
o-BPD	18	0.94	33.0	86.4	92.4	92.4
p-BPD	17	0.94	50.6	73.0	88.8	88.8
Spiro-OMeTAD	34	0.81	49.7	79.0	93.2	93.2
Spiro-TAD	25	0.85	41.8	66.2	78.2	78.3
TCTA	20	0.94	62.2	86.6	106.6	106.6
TPBi	21	0.87	24.6	68.3	72.6	72.6
TPyQB	25	0.85	33.9	70.1	77.8	77.9

Table S3: *Machine learning prediction of dynamic, static and total disorder for the HOMO level. The mean absolute validation error for the NN marks a lower bond for the disorder prediction. The squared sum of dynamic and static disorder should approximately match the total disorder.*

Molecule (LUMO)	Mean absolute error [meV]	r^2	Disorder static [meV]	Disorder dynamic [meV]	Disorder total [meV]	Squared Sum of dynamic and static disorder [meV]
a-NPD	14	0.97	22.1	95.1	97.6	97.6
B4PyMPM	20	0.97	87.7	113.3	143.2	143.3
B4PyPPM	28	0.93	88.8	107.9	139.7	139.7
m-BPD	36	0.91	91.3	116.0	147.6	147.7
mCP	15	0.97	38.0	102.2	109.0	109.1
NPB	14	0.96	27.3	93.9	97.7	97.8
o-BPD	31	0.93	80.4	122.0	146.0	146.1
p-BPD	34	0.92	93.2	118.0	150.3	150.4
Spiro-OMeTAD	35	0.88	81.2	99.9	128.7	128.7
Spiro-TAD	33	0.89	73.5	101.4	125.2	125.3
TCTA	32	0.94	106.0	134.4	171.1	171.2
TPBi	32	0.91	68.2	111.8	130.9	130.9
TPyQB	20	0.92	41.2	78.4	88.6	88.6

Table S4: *Machine learning prediction of dynamic, static and total disorder for the LUMO level. The mean absolute validation error for the NN marks a lower bond for the disorder prediction. The squared sum of dynamic and static disorder should approximately match the total disorder.*

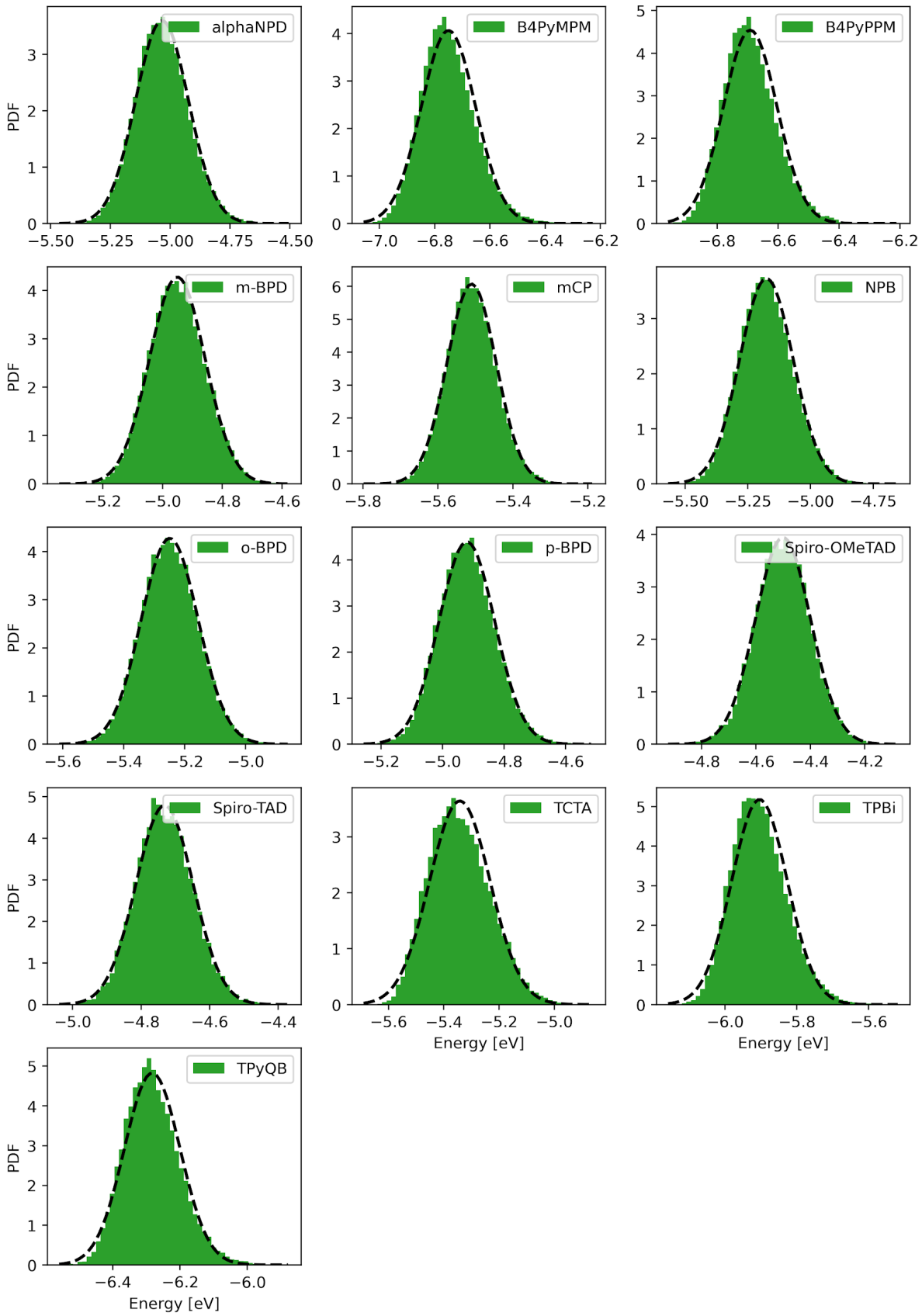

Figure S1: *Total DFT HOMO distribution for all molecules in this study. The probability density function is plotted versus energy. Total disorder.*

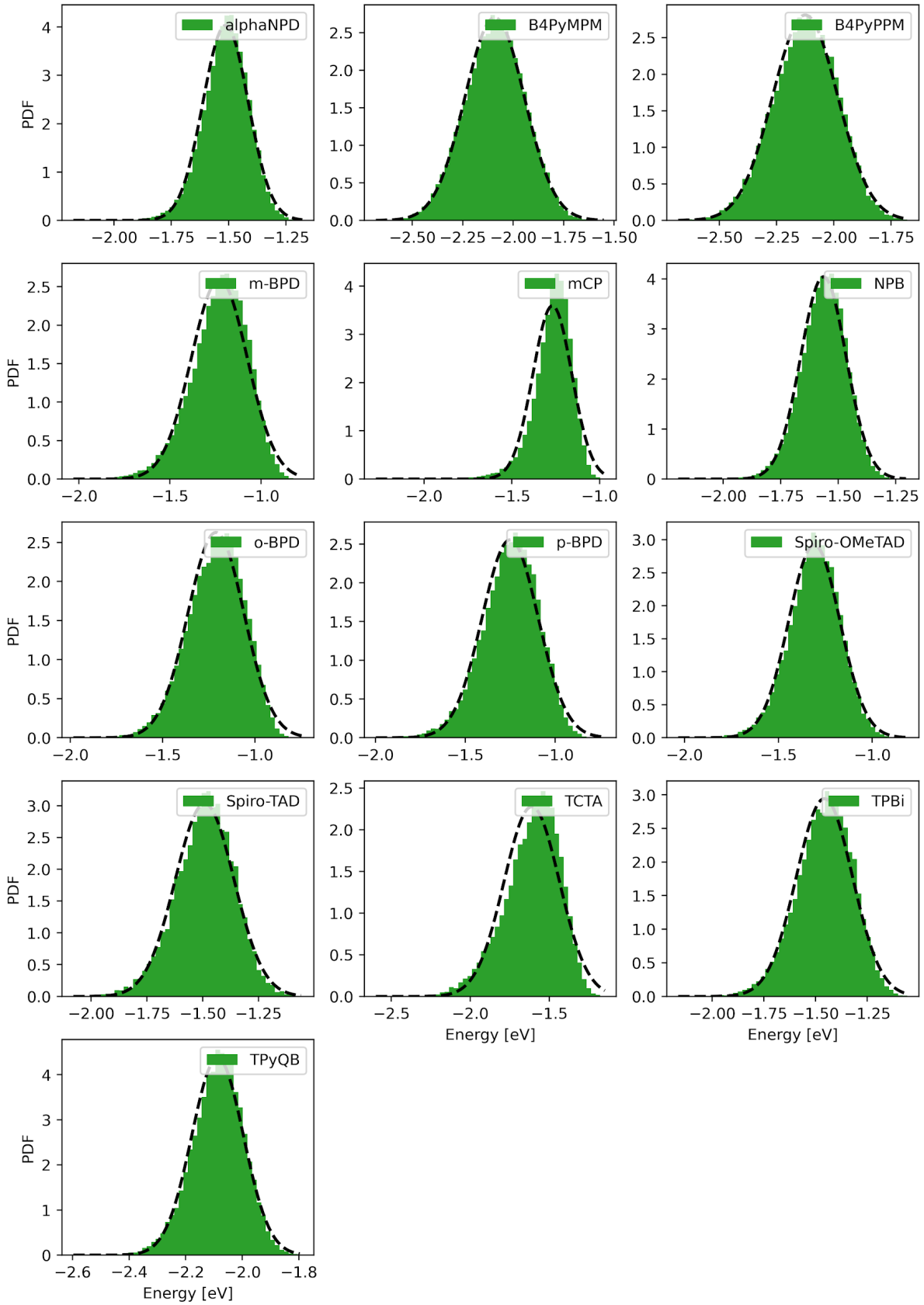

Figure S2: *Total DFT LUMO distribution for all molecules in this study. The probability density function is plotted versus energy. Total disorder.*

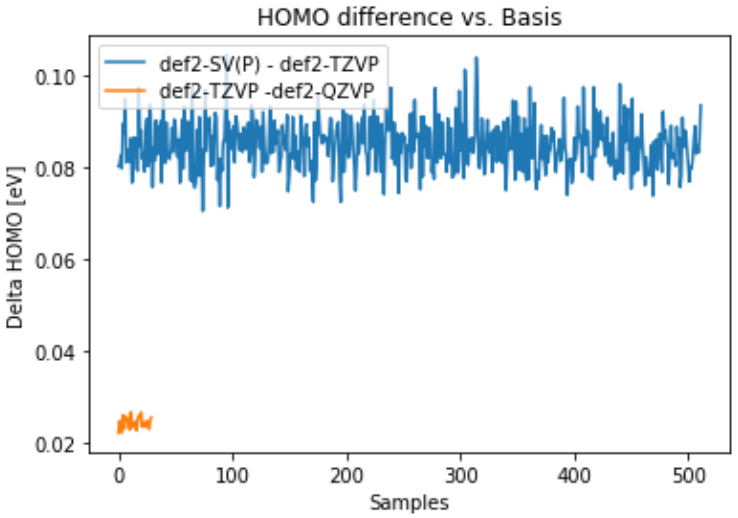

Figure S3: *DFT HOMO level difference of NPB for different Basis sets. The difference between def2-SV(P) and def2-TZVP and between def2-TZVP and def2-QZVP for random samples.*

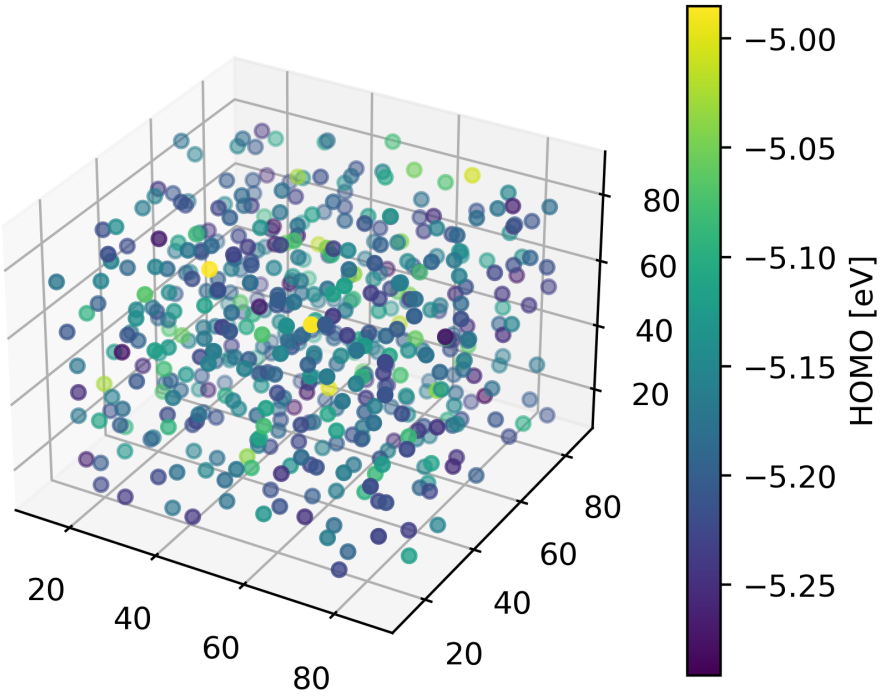

Figure S4: *3D plot of static (mean) HOMO distribution of NPB. The points represent the geometric center of a NPB molecule and the HOMO level is encoded by color. Points closer in the perspective view are less transparent.*

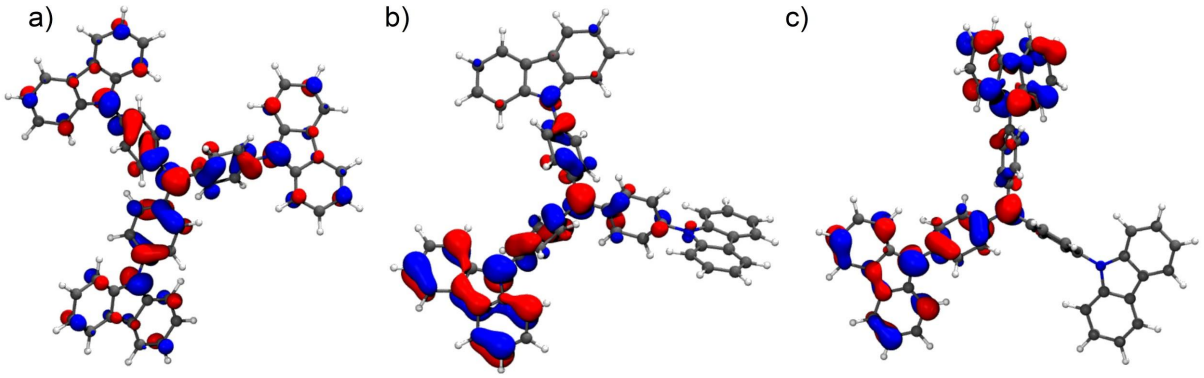

Figure S5: *Orbital of TCTA HOMO level. a) Vacuum orbital of an optimized structure. b) and c) Different conformers in the amorphous phase. The HOMO is nicely delocalized over the entire molecule but can be localized differently in c) or d).*

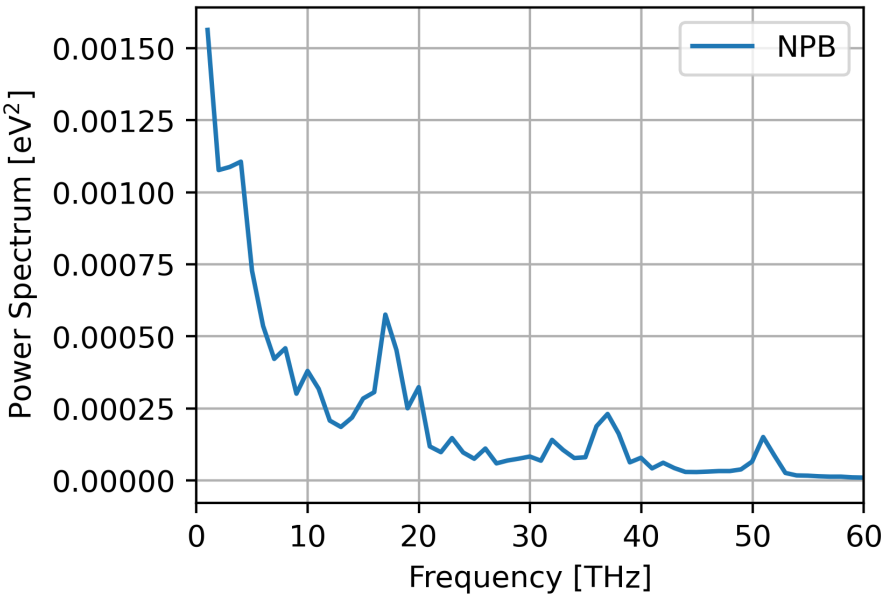

Figure S6: *Averaged FFT power spectrum of the small time step trajectories for NPB.*

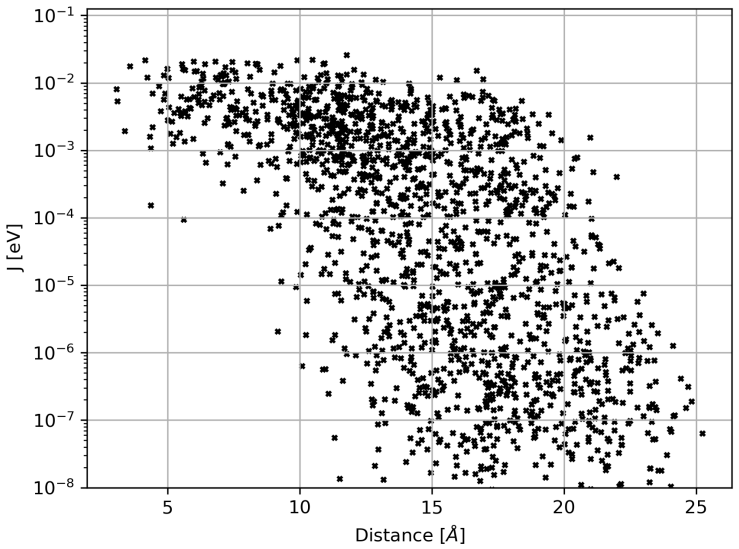

Figure S7: *Electronic coupling of NPB as a function of distance plotted for different orientations.*

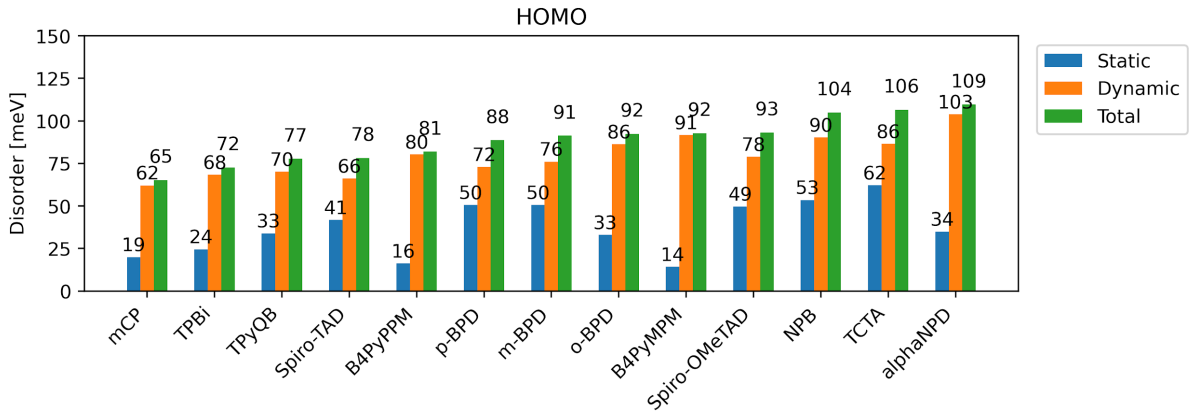

Figure S8: *Disorder calculated by the ML model of Table S3 for the HOMO level.*

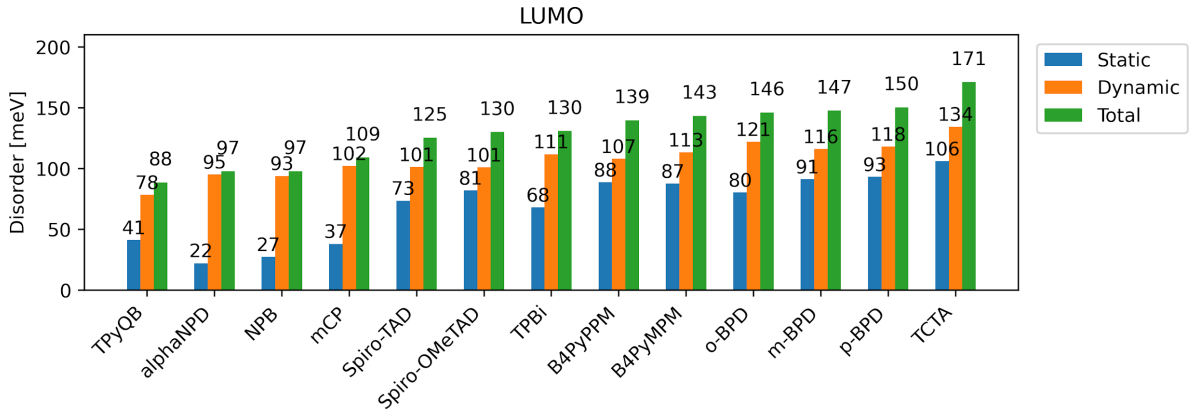

Figure S9: *Disorder calculated by the ML model of Table S3 for the LUMO level.*

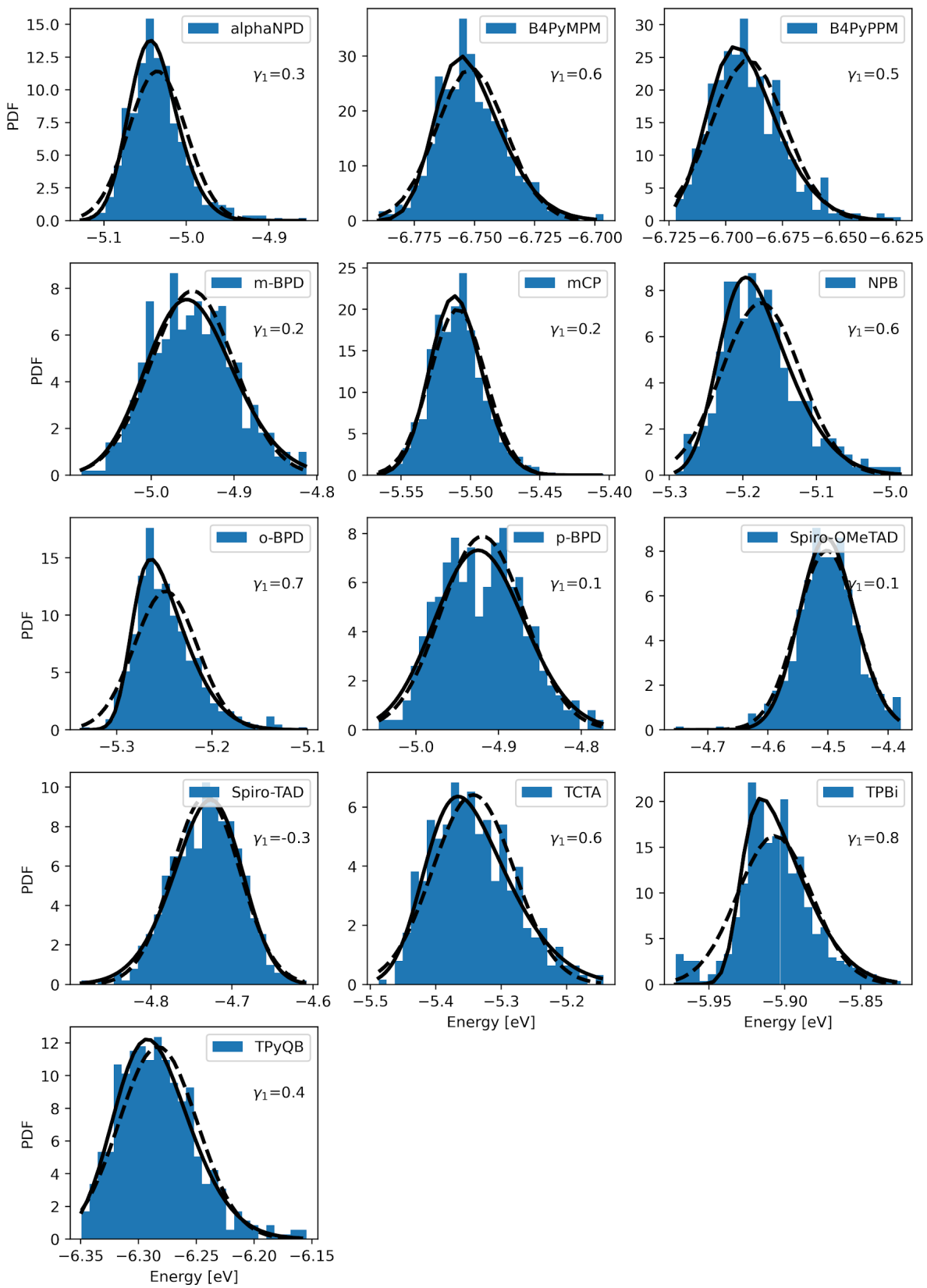

Figure S10: *HOMO static disorder distribution for all molecules estimated by the ML model. The dashed line is a gaussian fit and the solid line a skew normal distribution with skewness y_1 given as inset.*

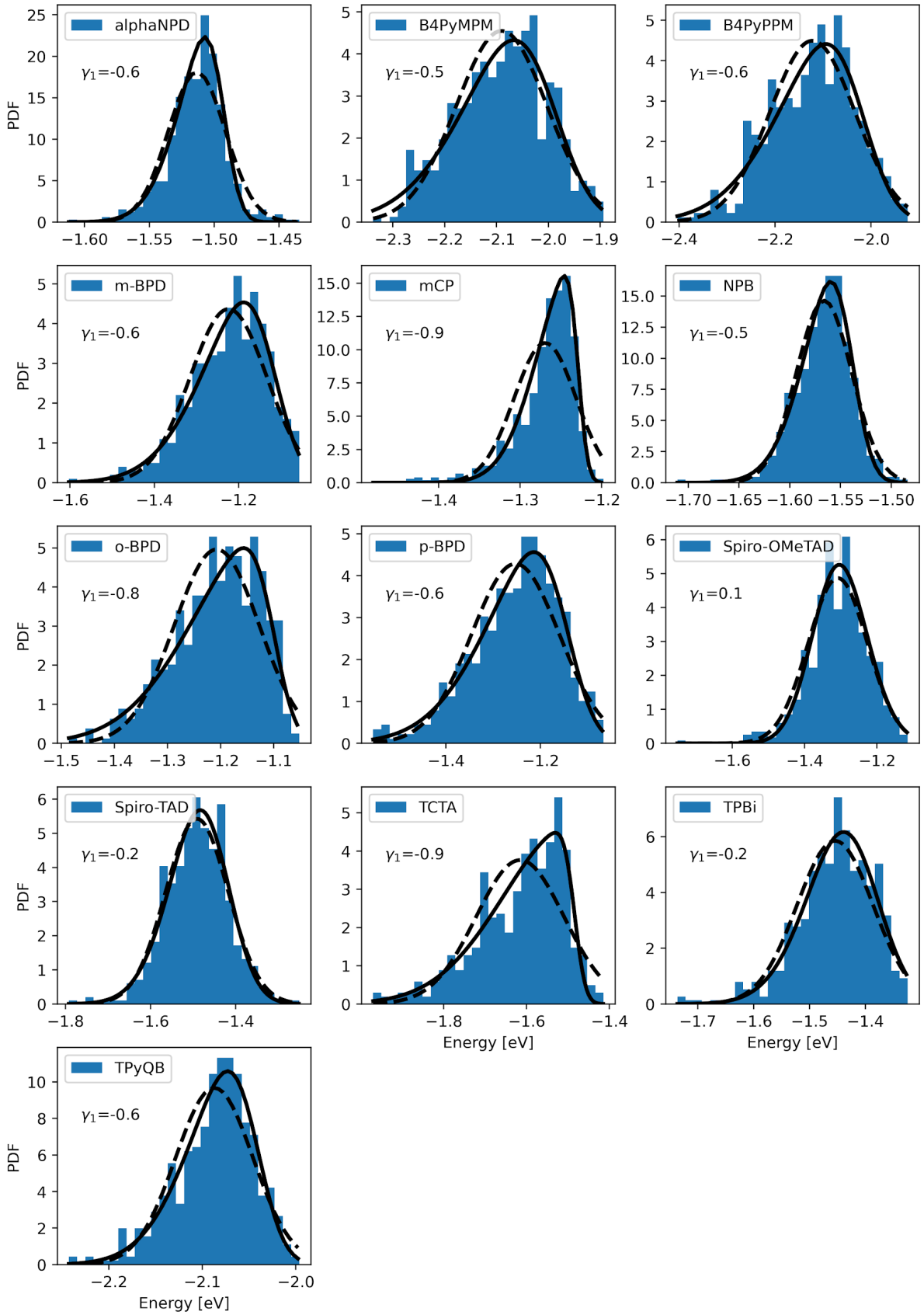

Figure S11: *LUMO static disorder distribution for all molecules estimated by the ML model.The dashed line is a gaussian fit and the solid line a skew normal distribution with skewness y_1 given as inset.*

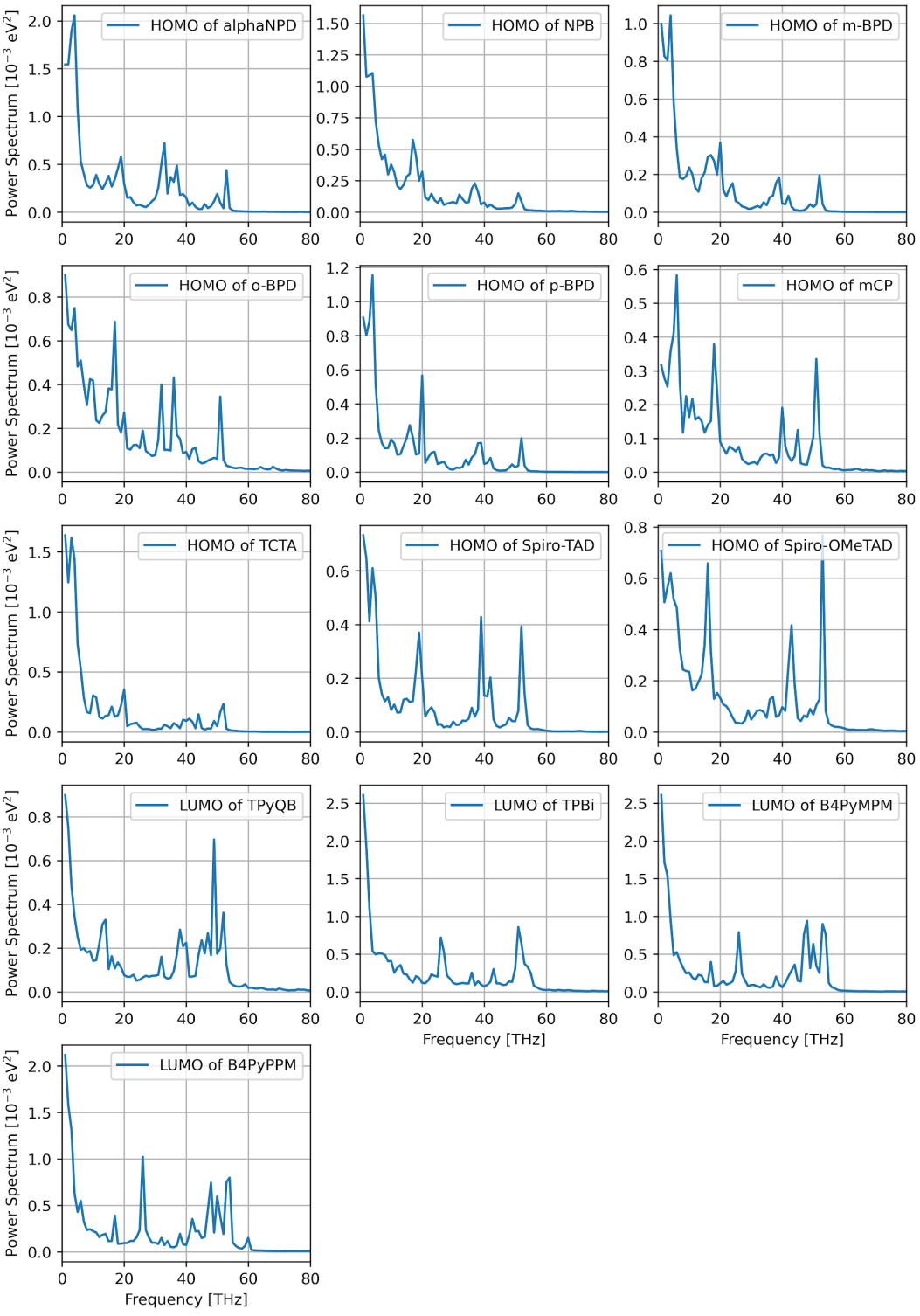

Figure S12: *Averaged power spectrum of the time-dependent HOMO/LUMO levels predicted by the ML model from the MD trajectories over 1000 fs with 1 fs time-step.*

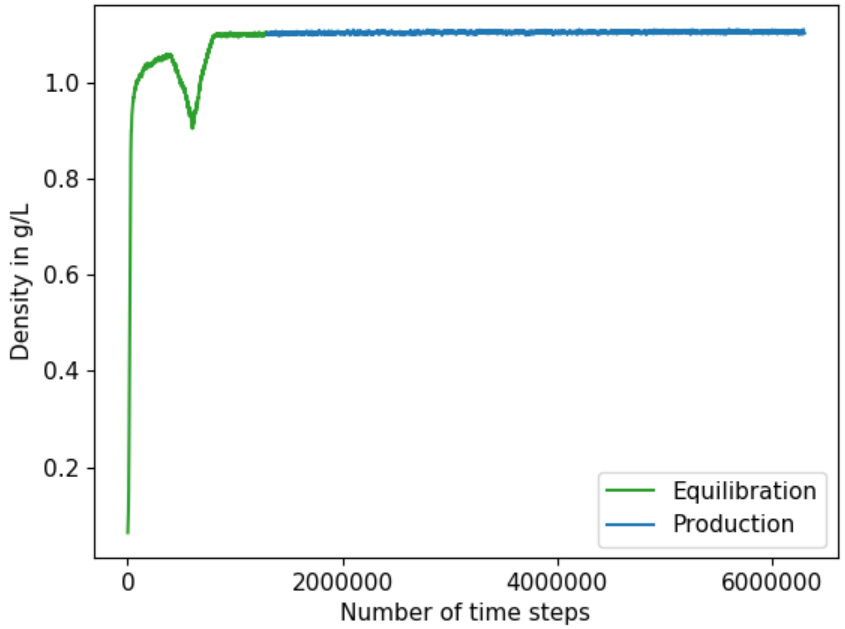

Figure S13: *Development of the mass density during the equilibration and production MD simulations of bulk NPB.*

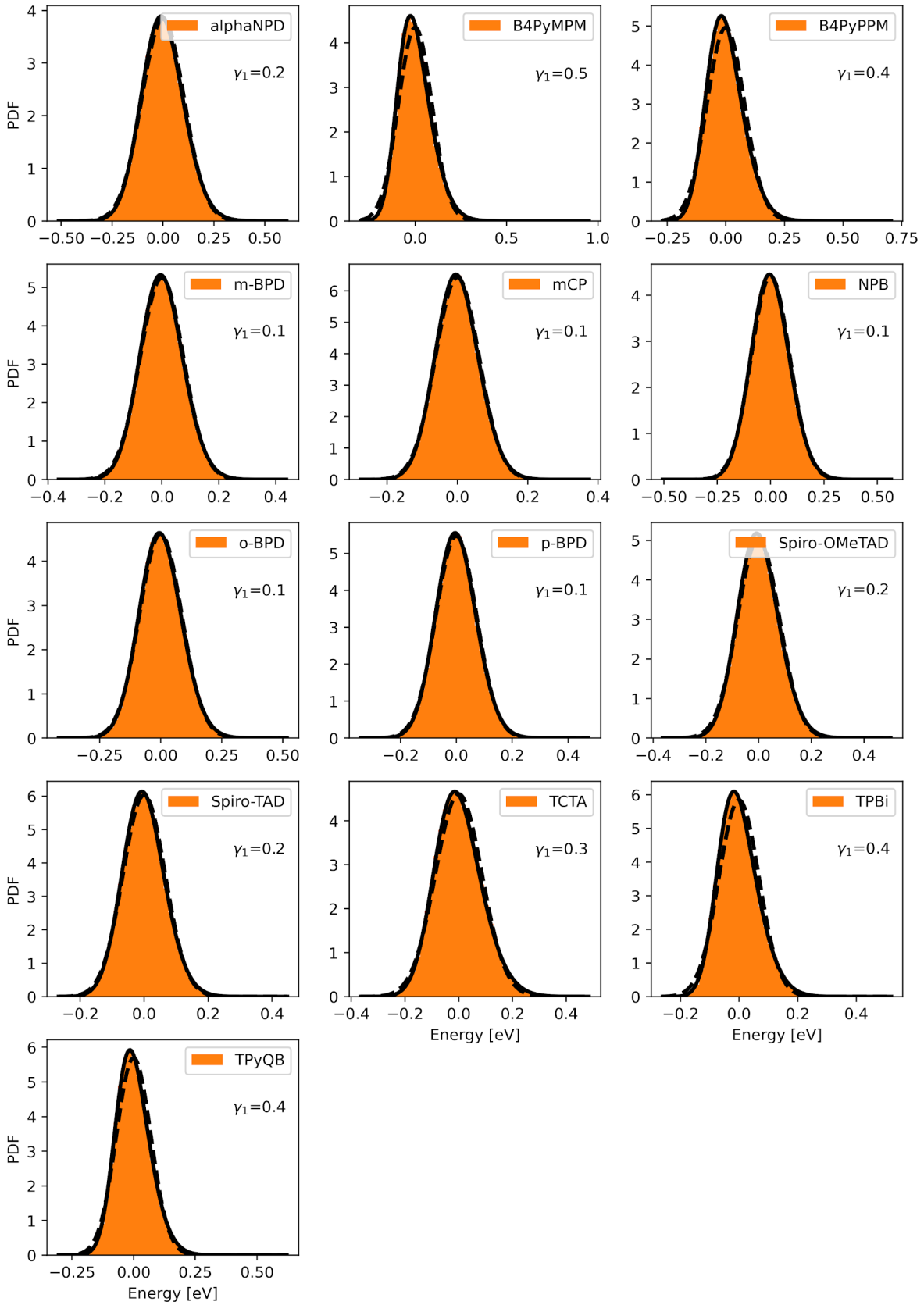

Figure S14: *HOMO dynamic disorder distribution for all molecules estimated by the ML model. The dashed line is a gaussian fit and the solid line a skew normal distribution with skewness y_1 given as inset.*

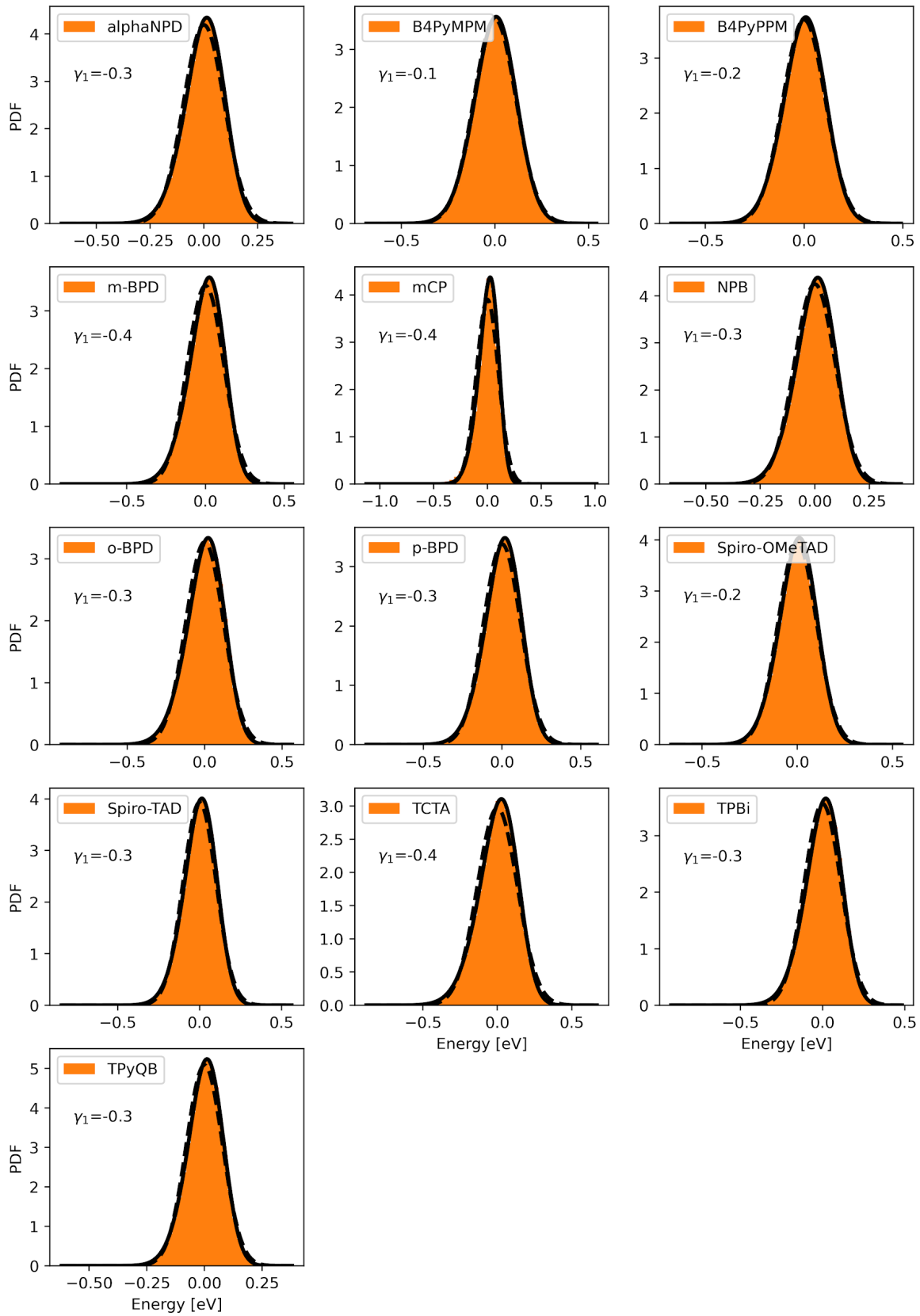

Figure S15: *LUMO dynamic disorder distribution for all molecules estimated by the ML model. The dashed line is a gaussian fit and the solid line a skew normal distribution with skewness y_1 given as inset.*

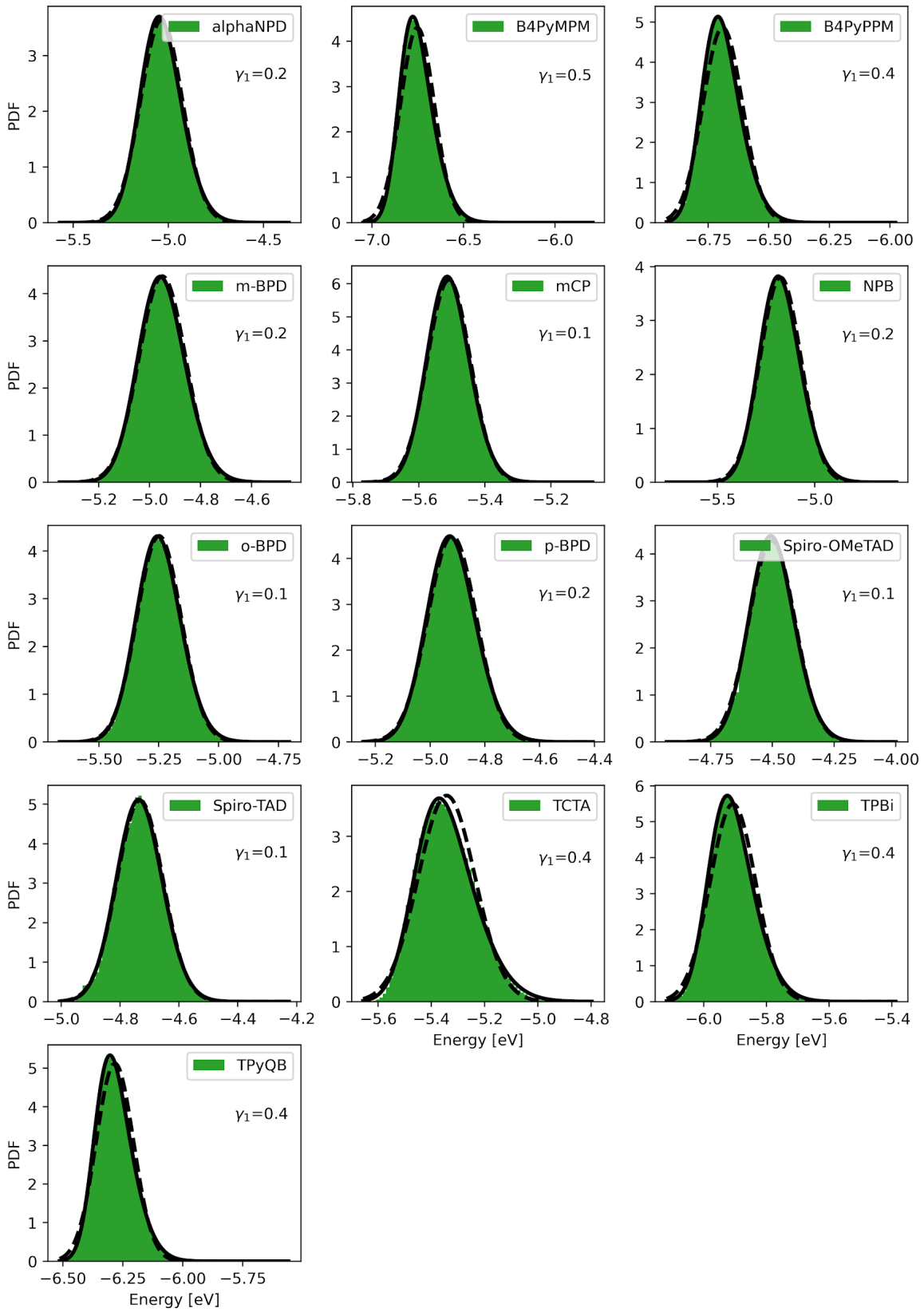

Figure S16: *HOMO total disorder distribution for all molecules estimated by the ML model. The dashed line is a gaussian fit and the solid line a skew normal distribution with skewness y_1 given as inset.*

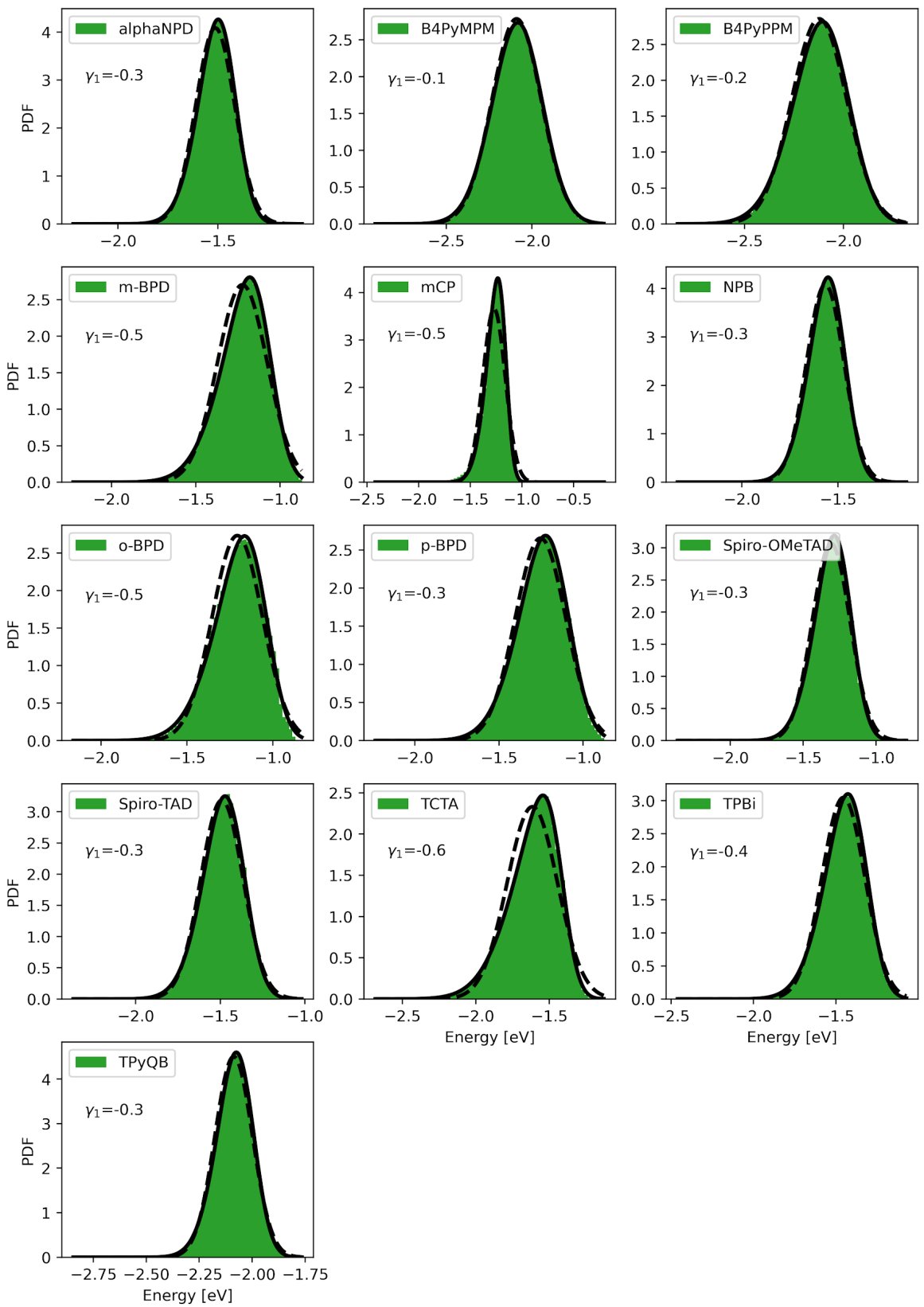

Figure S17: *LUMO total disorder distribution for all molecules estimated by the ML model. The dashed line is a gaussian fit and the solid line a skew normal distribution with skewness y_1 given as inset.*

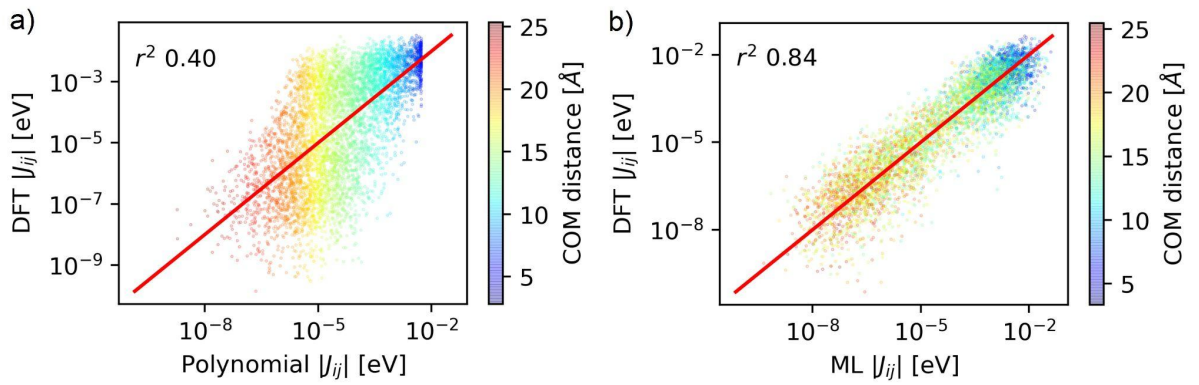

Figure S18: *Learned NPB coupling predictions log(|J_{ij}|) versus DFT reference. A total of 50k pairs were used for training and 5k pairs for validation. a) Polynomial Ridge Regression of the center of mass (COM) distance. The polynomial degree was 5 with α = 1.0 regularization. b) The same network architecture and training schedule from* ***Figure 2*** *was used but for pairs of NPB molecules instead of single molecules.*

Molecule (HOMO)	Simulated disorder [meV] static, (dynamic), electrostatic	Exp. disorder [meV]	Exp. Mobility [10^{-4} $cm^2V^{-1}s^{-1}$]
a-NPD	**35**, (104), ~76	90[1], 100-114[2]	3[3]
m-BPD	**51**, (76), ~58	105[4]	0.5[4]
mCP	**20**, (62), ~92	-	1.2[5]
NPB	**53**, (90), ~83	88-114[6], 76[7]	3[7]
o-BPD	**33**, (86), ~92	71[4]	6.5[4]
p-BPD	**51**, (73), ~64	75[4]	10[4]
Spiro-OMeTAD	**50**, (79), ~130	101[8]	2.0[8]
Spiro-TAD	**42**, (66), ~70	57[9], 80[8], 100[10]	3[10], 4[9], 5.0[8]
TCTA	**62**, (87), ~89	75[7], 90[10]	1.9[7]
Molecule (LUMO)	Simulated disorder [meV] static, (dynamic), electrostatic	Exp. disorder [meV]	Exp. Mobility [10^{-4} $cm^2V^{-1}s^{-1}$]
B4PyMPM	**88,** (113), ~131	76[11]	4.5[11]
TPBi	**68,** (112), ~166	-	0.33[12]
TPyQB	**41,** (78), ~104	-	33[13]

Table S5: *Simulated conformational disorder from this work compared to experimental energetic disorder from mobility measurements in literature.*[14] *It is to note, that the disorder relevant for experiment* $\boldsymbol{\sigma}_{exp}^2 = \boldsymbol{\sigma}_s^2 + \boldsymbol{\sigma}_p^2$ *is a combination of static conformational* $\boldsymbol{\sigma}_s$ *and electrostatic disorder* $\boldsymbol{\sigma}_p$*. The electrostatic disorder* $\boldsymbol{\sigma}_p$ *is not a focus of this work but was estimated by simulating polarization effects using QuantumPatch*[15] *embeddings on the same morphologies and assuming* $\boldsymbol{\sigma}_p^2 = \boldsymbol{\sigma}^2 - \boldsymbol{\sigma}_c^2$*, where the conformational disorder is composed of* $\boldsymbol{\sigma}_c^2 = \boldsymbol{\sigma}_s^2 + \boldsymbol{\sigma}_d^2$*. We tried to select time-of-flight (TOF) mobility measurements from literature, if available.*

References

(1) Rohloff, R.; Kotadiya, N. B.; Crăciun, N. I.; Blom, P. W. M.; Wetzelaer, G. a. H. Electron and Hole Transport in the Organic Small Molecule α-NPD. *Appl. Phys. Lett.* **2017**, *110* (7), 073301. https://doi.org/10.1063/1.4976205.

(2) van Mensfoort, S. L. M.; Shabro, V.; de Vries, R. J.; Janssen, R. a. J.; Coehoorn, R. Hole Transport in the Organic Small Molecule Material α-NPD: Evidence for the Presence of Correlated Disorder. *J. Appl. Phys.* **2010**, *107* (11), 113710. https://doi.org/10.1063/1.3407561.

(3) Nguyen, N. D.; Schmeits, M.; Loebl, H. P. Determination of Charge-Carrier Transport in Organic Devices by Admittance Spectroscopy: Application to Hole Mobility in a-NPD. *Phys. Rev. B* **2007**, *75* (7), 075307. https://doi.org/10.1103/PhysRevB.75.075307.

(4) Okumoto, K.; Wayaku, K.; Noda, T.; Kageyama, H.; Shirota, Y. Amorphous Molecular Materials: Charge Transport in the Glassy State of N,N′-Di(Biphenylyl)-N,N′-Diphenyl-[1,1′-Biphenyl]-4,4′-Diamines. *Synth. Met.* **2000**, *111–112*, 473–476. https://doi.org/10.1016/S0379-6779(99)00421-X.

(5) Hsiao, C.-H.; Liu, S.-W.; Chen, C.-T.; Lee, J.-H. Emitting Layer Thickness Dependence of Color Stability in Phosphorescent Organic Light-Emitting Devices. *Org. Electron.* **2010**, *11* (9), 1500–1506. https://doi.org/10.1016/j.orgel.2010.06.008.
(6) Chu, T.-Y.; Song, O.-K. Apparent Thickness Dependence of Mobility in Organic Thin Films Analyzed by Gaussian Disorder Model. *J. Appl. Phys.* **2008**, *104* (2), 023711. https://doi.org/10.1063/1.2959825.
(7) Chan, C. Y. H.; Tsung, K. K.; Choi, W. H.; So, S. K. Achieving Time-of-Flight Mobilities for Amorphous Organic Semiconductors in a Thin Film Transistor Configuration. *Org. Electron.* **2013**, *14* (5), 1351–1358. https://doi.org/10.1016/j.orgel.2013.02.007.
(8) Poplavskyy, D.; Nelson, J. Nondispersive Hole Transport in Amorphous Films of Methoxy-Spirofluorene-Arylamine Organic Compound. *J. Appl. Phys.* **2002**, *93* (1), 341–346. https://doi.org/10.1063/1.1525866.
(9) Saragi, T. P. I.; Fuhrmann-Lieker, T.; Salbeck, J. Comparison of Charge-Carrier Transport in Thin Films of Spiro-Linked Compounds and Their Corresponding Parent Compounds. *Adv. Funct. Mater.* **2006**, *16* (7), 966–974. https://doi.org/10.1002/adfm.200500361.
(10) Kotadiya, N. B.; Mondal, A.; Xiong, S.; Blom, P. W. M.; Andrienko, D.; Wetzelaer, G.-J. A. H. Rigorous Characterization and Predictive Modeling of Hole Transport in Amorphous Organic Semiconductors. *Adv. Electron. Mater.* **2018**, *4* (12), 1800366. https://doi.org/10.1002/aelm.201800366.
(11) Sasabe, H.; Tanaka, D.; Yokoyama, D.; Chiba, T.; Pu, Y.-J.; Nakayama, K.; Yokoyama, M.; Kido, J. Influence of Substituted Pyridine Rings on Physical Properties and Electron Mobilities of 2-Methylpyrimidine Skeleton-Based Electron Transporters. *Adv. Funct. Mater.* **2011**, *21* (2), 336–342. https://doi.org/10.1002/adfm.201001252.
(12) Wu, I.-W.; Wang, P.-S.; Tseng, W.-H.; Chang, J.-H.; Wu, C.-I. Correlations of Impedance–Voltage Characteristics and Carrier Mobility in Organic Light Emitting Diodes. *Org. Electron.* **2012**, *13* (1), 13–17. https://doi.org/10.1016/j.orgel.2011.09.016.
(13) Ahmed, E.; Earmme, T.; Jenekhe, S. A. New Solution-Processable Electron Transport Materials for Highly Efficient Blue Phosphorescent OLEDs. *Adv. Funct. Mater.* **2011**, *21* (20), 3889–3899. https://doi.org/10.1002/adfm.201100848.
(14) Li, H.; Li, C.; Duan, L.; Qiu, Y. Charge Transport in Amorphous Organic Semiconductors: Effects of Disorder, Carrier Density, Traps, and Scatters. *Isr. J. Chem.* **2014**, *54* (7), 918–926. https://doi.org/10.1002/ijch.201400057.
(15) Friederich, P.; Meded, V.; Symalla, F.; Elstner, M.; Wenzel, W. QM/QM Approach to Model Energy Disorder in Amorphous Organic Semiconductors. *J. Chem. Theory Comput.* **2015**, *11* (2), 560–567. https://doi.org/10.1021/ct501023n.